



2,4-Dichlorophenol removal from water by walnut shells-based biochar

Xuan Zhou^a, Xinyuan Li^a, Li Guo^a, Xiuying Liu^{b,*}, Yangshuo Liu^{c,d,e,*}

^aSchool of Chemistry and Environmental Engineering, Wuhan Institute of Technology, 430205, China, emails: hbzhoux@sina.com (X. Zhou), ynlxy06@163.com (X. Li), liguo@whu.edu.cn (L. Guo)

^bSchool of Chemistry and Chemical Engineering, Wuhan Textile University, Wuhan 430073, China, email: liuxiuying@wtu.edu.cn

^cKey Laboratory of Advanced Textile Materials and Manufacturing Technology, Ministry of Education (Zhejiang Sci-Tech University), Hangzhou 310018, China, email: liuyangshuo8858@163.com

^dZhejiang Provincial Key Laboratory of Fiber Materials and Manufacturing Technology (Zhejiang Sci-Tech University), Hangzhou 310018, China

^eState Key Laboratory of New Textile Materials and Advanced Processing Technologies, Wuhan Textile University, Wuhan 430073, China

Received 2 August 2021; Accepted 21 January 2022

ABSTRACT

Walnut shell, as a biomass waste, was used as material to prepare walnut shell biochar (WSB), nitrogen-doped biochar (NB), Hummers-modified biochar (HB), and alkali-activated biochar (AB). The biochars were used as adsorbents for the removal of the hazardous and poorly degradable 2,4-dichlorophenol (2,4-DCP) in water. The structures and morphologies of the biochars were analyzed by Raman spectra, Fourier transform infrared spectroscopy, and scanning electron microscopy. The pore structures of AB and WSB were compared using Brunauer–Emmett–Teller analysis and AB had shown a mesopore structure with a smaller pore size and larger specific surface area. The adsorption behaviors of 2,4-DCP on WSB, NB, HB, and AB were studied. The adsorption followed the pseudo-second-order kinetic model and Langmuir isotherm model indicating chemical and monolayer adsorption process. The adsorption mechanism was discussed. AB exhibited the highest removal rate for 2,4-DCP (96.5%) and adsorption capacity (240.4 mg/g), due to its larger specific surface area and the aromatic compounds formed during pyrolysis. The removal rate was 4.2 times that of the commercial activated carbon. In brief, AB had the potential to be applied as a low-cost and effective adsorbent for 2,4-DCP removal from water. This present work will provide a foundation for the treatment of chlorophenol pollutants in wastewater and for the resource utilization of walnut shells.

Keywords: Walnut shell; Biochar; Adsorption; 2,4-Dichlorophenol; Modification

1. Introduction

The annual world production of walnuts is over 3.7 million tons and the production in China is over 1.06 million tons [1]. Therefore, walnut shells are abundant in China. However, the shells are mostly discarded or burned as biomass wastes. It not only causes a waste of resources but also pollutes the environment [2–4]. In view of valorization, walnut shells have been studied as regards chemical

composition, fractionation behavior, anatomical features, and so on [1,5]. It is highly lignified with the lignin content between 27.4 and 52.3 wt.%, the cellulose content between 25.6%–34.5%, and the hemicelluloses content of 22.1% [1].

Biomass waste, such as forestry wastes and crop residues, are appropriate materials for biochar production. As a kind of crop residue, walnut shell offers several advantages, which includes high availability, low cost of raw materials, and simplicity of disposal [6,7]. Biochar is a carbon-rich

* Corresponding authors.

material that was prepared by thermal decomposition of biomass under oxygen-limited conditions. Compared with activated carbon, it is generally less carbonized and more hydrogen with oxygen remain in its structure [8]. Moreover, biochar requires less investment and is mainly used in soil conditioning and remediation.

In recent years, many researchers have shown an increased interest in the application of biochar as an adsorbent in water treatment for removing inorganic and organic contaminants from water [8,9]. Biochar exhibited good removal efficiencies in the majority of studies. Modifications of the biochar for enhanced adsorption effect were also explored. The main modification methods included the heteroatom doping method [10,11], the Hummers method [12], and the acid/alkali activation method [13,14].

2,4-Dichlorophenol (2,4-DCP) is hazardous, but it is widely used in the synthesis of pesticides, herbicides, nylon, plastics, and dyes in the field of industry [15–17]. It easily penetrates the groundwater through the soil, resulting in pollution in rivers, lakes, and groundwater. What is more, 2,4-DCP has poor biodegradability and a long degradation cycle in the water body [18,19], due to its stable conjugated structure formed by benzene ring and chlorine atoms.

At present, the commonly used methods for chlorophenol removal include biological treatment [17,19,20], chemical redox method [21,22], physical adsorption [8,17,23], etc. The biological method is more suitable for the treatment of low concentrations of chlorophenol wastewater. Chemical redox methods have disadvantages including high consumption, high costs, and the possibility of causing secondary environmental problems. As compared to biological and chemical methods, adsorption methods are simpler, more efficient, and have been attracting considerable interest. For example, Allwar and Syamsurizal [24] reported the removal of 2-chlorophenol through adsorption by rice husk activated carbon prepared by $\text{ZnCl}_2/\text{H}_3\text{PO}_4$ activation, and the removal rate was 77.6%. Batool et al. [15] design a SnO_2 templated with grapefruit peel carbon as a nanocomposite for enhanced adsorption of 2,4-DCP and the maximum adsorption capacity was 45.95 mg/g. Ren et al. [25] used activated carbon prepared from cat-tail fiber via phosphoric acid activation as adsorbent. The adsorbent had a porous structure with a large surface area of 890.27 m^2/g and the maximum removal rate was about 85% for 2,4-DCP and 95% for 2,4,6-TCP.

Currently, biochar materials derived from waste biomass were also used for phenol removal [8]. Biochars prepared from pyrolysis of rice-husks and corncob exhibited a high phenol adsorption capacity of 589 mg/g [26]. Adsorption of 2,4-dichlorophenol on paper sludge/wheat husk biochar could reach 99.95% under optimum adsorption conditions [27]. Wu and Chen [28] investigated the effect of fulvic acid coating on biochar surface on the sorption properties towards 4-chlorophenol. Liu et al. [23] studied the adsorption behavior of 2,4-DCP by rice straw biochar modified with cetyltrimethylammonium bromide. The maximum adsorption capacity was 59.81 mg/g.

Walnut shell-based biochar had been produced by pyrolysis and modified by metal oxides and basic functional groups. The modified biochar was used as a catalyst for the hydrolysis of carbon disulphide (CS_2) and carbonyl sulphide (COS) at low temperatures. Upon modification, the catalytic activity was significantly improved, yielding a 100% removal rate of CS_2 and COS after 330 and 240 min, respectively [29]. Additionally, walnut shell-based biochar had been produced by hydrothermal carbonization and modified by nitric acid for the adsorption of methylene blue and malachite green. The removal rates at 25°C for 24 h were both about 60% [6].

Herein, walnut shell biochar (WSB) was prepared by a one-step pyrolysis method. Furthermore, three different modification methods were used to prepare nitrogen-doped biochar (NB), Hummers-modified biochar (HB), and alkali-activated biochar (AB). These walnut shell-based biochar materials were analyzed by Raman, Fourier transform infrared spectroscopy (FT-IR), scanning electron microscopy (SEM), and Brunauer–Emmett–Teller (BET). The static adsorption of 2,4-DCP on the biochars was then investigated by studying the adsorption isotherms, kinetics, and mechanism. The experimental flow chart of this study is shown in Fig. 1.

2. Materials and methods

2.1. Materials

2,4-Dichlorophenol, sodium nitrate (NaNO_3), potassium permanganate (KMnO_4), sodium hydroxide (NaOH), ethyl violet, hydrogen peroxide (H_2O_2), and all other reagents are analytically pure. The walnuts were produced in China and purchased from the supermarket.

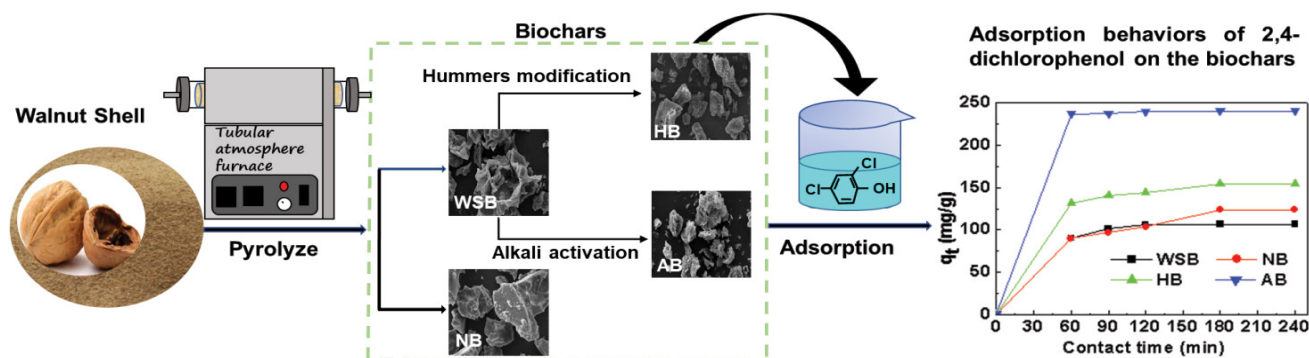


Fig. 1. Experimental flowchart.

2.2. Preparation of walnut shell biochar

Walnut shell powder (15 g) was washed 3 times with deionized water and dried overnight. Subsequently, it was placed into a tubular atmosphere furnace which was heated up to 600°C at a 5°C/min heating rate. The pyrolysis was conducted at 600°C for 2 h under an N₂ atmosphere. After cooling down to room temperature, the product was immersed in 100 mL of hydrochloric acid solution (2 mol/L) for 12 h to remove the residues. The biochar was then washed with deionized water until pH = 7.0 and dried at 80°C overnight. The resulting material was named WSB.

2.3. Preparation of nitrogen-doped biochar

The preparation of NB was similar to that of WSB except that the dried walnut shell powder was impregnated with ethyl violet to dope the nitrogen atoms before pyrolysis.

2.4. Modification of WSB through the Hummers method (Preparation of HB)

WSB was mixed evenly with an equal amount of NaNO₃ in the concentrated sulfuric acid solution in an ice bath. Then an equal amount of KMnO₄ was divided into five parts and slowly added into the mixture successively. The mixture was heated at 35°C for 6 h and then deionized water was added. The mixture was heated at 95°C for a further 15 min. Subsequently, 30% hydrogen peroxide was added to the mixture to produce a yellow solution. Then 10% hydrochloric acid was added and the mixture was stirred at room temperature for 12 h. The resulting material was washed with deionized water to be neutralized and dried. The product was named HB.

2.5. Alkali activation of WSB (Preparation of AB)

WSB and NaOH were evenly mixed in a nickel crucible at a mass ratio of 1:4. The mixture was pyrolyzed at 650°C and carbonized for 50 min. The resulting material was washed with deionized water to be neutralized and dried. The obtained biochar was named AB.

2.6. Adsorption experiment

The adsorbent was placed into 100 mL of 2,4-DCP solution (50 mg/L) and the dosage of the adsorbent was 0.1 g/L. The mixture was magnetically stirred at room temperature for 4 h. The supernatant solution was centrifugated and the concentration of 2,4-DCP was calculated from the absorbance at 286 nm recorded by a UV-Visible spectrometer. The equilibrium adsorption capacity q_e (mg/g) of the adsorbent and the removal rate (%) were calculated according to Eqs. (1) and (2), respectively:

$$q_e = \frac{(C_0 - C_e)V}{m} \quad (1)$$

$$\text{Removal rate} = \frac{C_0 - C_e}{C_0} \times 100\% \quad (2)$$

where C_0 (mg/L) and C_e (mg/L) represent the initial concentration of 2,4-DCP in solution and the concentration after adsorption equilibrium, respectively. V (mL) and m (g) represent the volume of solution and the mass of adsorbent, respectively.

2.7. Adsorption kinetics

To evaluate the adsorption kinetics, a certain amount of biochar was added into 100 mL 2,4-DCP solution (50 mg/L). The mixed solution was shaken at 150 rpm for a period of time (30–240 min). The concentration of 2,4-DCP was determined from the absorbance at 286 nm. The pseudo-first-order adsorption kinetic model, pseudo-second-order kinetic model, and intraparticle diffusion model were used to fit the data of 2,4-DCP adsorption, respectively. The equation is as follows [30]:

$$\frac{dq_t}{dt} = k_1(q_e - q_t) \quad (3)$$

where q_t (mg/g) is the adsorption amount at time t , k_1 (g/(mg min)) is the adsorption rate constant of the pseudo-first-order model.

When $q_t = 0$ and $t = 0$, Eq. (3) can be expressed:

$$\ln(q_{1e} - q_t) = \ln q_{1e} - k_1 t \quad (4)$$

$$\frac{t}{q_t} = \frac{1}{k_2 q_{2e}^2} + \frac{t}{q_{2e}} \quad (5)$$

$$q_t = k_{id} t^{0.5} + C \quad (6)$$

where q_{1e} and q_{2e} (mg/g) represent the equilibrium adsorption capacity of the pseudo-first-order and pseudo-second-order adsorption kinetic model, respectively. k_2 (g/(mg min)) is the adsorption rate constant of pseudo-second-order equation. k_{id} (mg/(g min^{1/2})) is the internal diffusion rate constant. C (mg/g) is the internal diffusion model parameter.

2.8. Adsorption isotherm

0.02 g of biochar was added to 100 mL of solutions containing 2,4-DCP at different concentrations (0, 10, 20, 30, 40, and 50 mg/L). The mixture was shaken at 150 rpm for 240 min to reach equilibrium and then it was filtered and the absorbance was measured.

In this experiment, Freundlich [Eq. (7)] and Langmuir [Eq. (8)] models were used to fit the data of 2,4-DCP adsorption, as follows [31,32]:

$$\ln q_e = \ln k_f + \frac{\ln C_e}{n} \quad (7)$$

$$\frac{C_e}{q_e} = \frac{1}{k_L q_m} + \frac{C_e}{q_m} \quad (8)$$

where q_e and q_m (mg/g) are the equilibrium adsorption capacity and saturated adsorption capacity, respectively. k_F and k_L are the Freundlich and Langmuir adsorption coefficients, respectively. C_e (mg/L) is the equilibrium concentration of 2,4-DCP in the solution, $1/n$ is the Freundlich index.

The equilibrium constant (R_L) equation [Eq. (7)] is as follows:

$$R_L = \frac{1}{1 + k_L C_0} \quad (9)$$

where C_0 (mg/L) represents the initial concentration of 2,4-DCP in solution.

2.9. Characterization and instrument

Raman spectra were recorded with DXR Raman Microscope (Thermo Fisher, USA). FT-IR were recorded using Nicolet 6700 FT-IR Spectrometer (Thermo Fisher, USA). The surface morphology of biochar was tested by scanning electron microscopy (SEM, JSW-5510LV, Japan Electronics Corporation, Japan). The surface area and pore structure of biochars were analyzed from N_2 isotherm at 78 K using automatic specific surface area and porosity analyzer (MIKE 2020, USA). The concentration of 2,4-DCP in the solution was determined using a UV-Visible spectrometer (YK-752, Shanghai Yoke Instrument Co., Ltd., China). The correlation coefficient of the standard curve was 0.999. A tubular atmosphere furnace (T1250S, Henan Chengjin Instrument Equipment Co., Ltd., China) was used for pyrolysis.

3. Results and discussion

3.1. Structure analysis by Raman spectrum

Raman spectrum was used to analyze the structure of biochars (Fig. 2). The absorption peak at 1,342–1,368 cm^{-1}

was considered to be the D peak representing the carbon atom defect. The characteristic absorption peak at 1,582–1,596 cm^{-1} was considered to be the G peak representing the in-plane bond-stretching motion of the pairs of C sp^2 atoms. The intensity ratio of I_D to I_G (I_D/I_G) is usually used to characterize the defect intensity [33]. I_D/I_G of WSB, NB, HB, and AB were 0.725, 0.811, 0.729, and 1.108, respectively. By comparison, the change between WSB and AB was obvious. The higher value suggested that the structure of AB tended to be disordered. The disordered structure may lead to an increase in specific surface area [34].

3.2. Functional group analysis

The functional groups of WSB, NB, HB, and AB were analyzed by infrared spectroscopy, as shown in Fig. 3. The main absorptions they all exhibited included those at about 3,448, 2,921, and 1,079 cm^{-1} , respectively. The peak near 3,448 cm^{-1} can be assigned to hydroxyl groups from cellulose, hemicellulose, and lignin in the biomass. The bands at 2,921 cm^{-1} belonged to C–H stretching vibrations in methyl and methylene groups. The absorptions at around 1,079 cm^{-1} corresponded to C–O bonds in phenolic, alcohol, and other functional groups. In other words, there were hydrogen and oxygen remaining in the biochar.

For NB, a new peak appeared at 1,623 cm^{-1} , which was contributed by N–H vibrations. It suggested that NB was doped with nitrogen atoms by ethyl violet. As to HB, new bands appeared at 1,619 and 1,708 cm^{-1} which were the characteristic peaks of the C=O group. The bands indicated that the material was oxidized by $KMnO_4$. AB showed a new band at 1,415 cm^{-1} that can be assigned to bending vibration absorption of C–C stretching of the aromatic ring [5]. Aromatic hydrocarbons and their derivatives formed during pyrolysis process and the content is generally dependent on the applied feedstock, pyrolysis temperature, and pyrolysis time, as reported by previous literature [35,36]. In

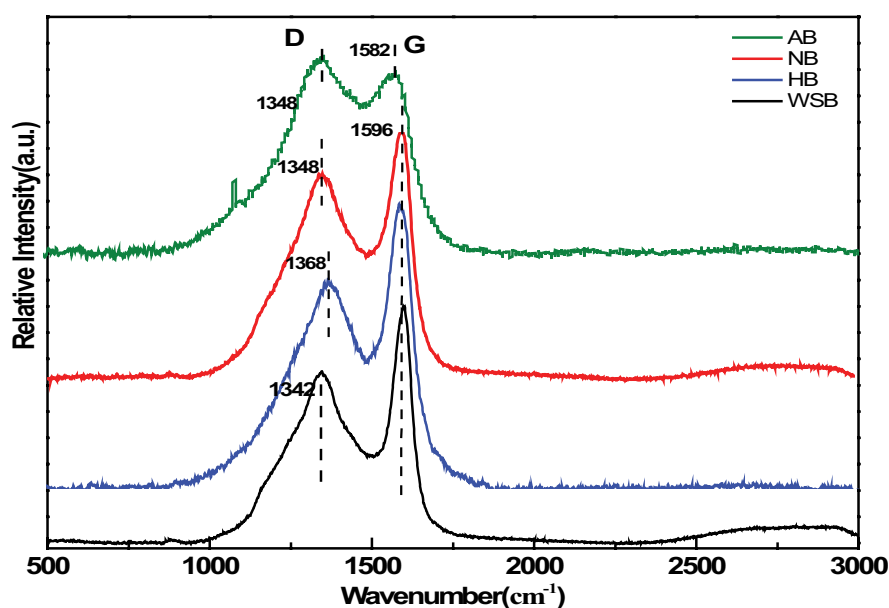


Fig. 2. Raman pattern of WSB, NB, HB, and AB.

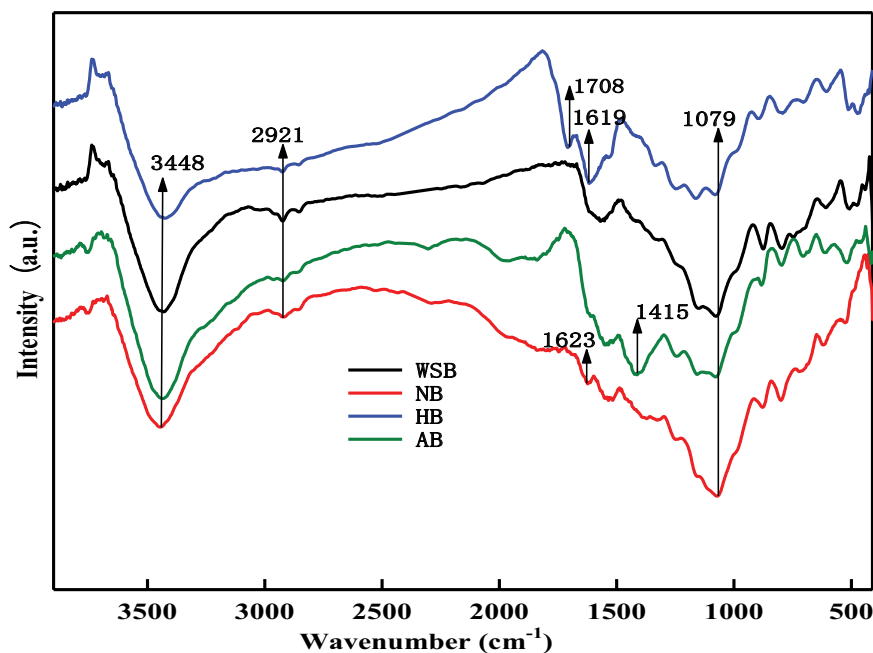


Fig. 3. FT-IR spectra of WSB, NB, HB, and AB.

conclusion, the band changes confirmed the modification of biochar and indicated that the second pyrolysis process with NaOH at higher temperature than the first one produced the aromatic hydrocarbons and their derivatives which were not found in WSB.

3.3. Surface and cross-section morphologies

The SEM images of the surface and cross-section of biochars are shown in Fig. 4. Compared with WSB (Fig. 4a and e), NB had a blocky structure with a rough surface (Fig. 4b and f), while HB had a massive and layered structure with some cracks and holes (Fig. 4c and g). The porous structure was formed during the carbonization process in which the Scholl reaction occurred under KMnO_4 and the polymeric PAHs was produced [37]. As to AB (Fig. 4d and h), the layered and porous structure was more obvious. The structure was formed probably due to the destruction of material by strong alkaline under pyrolysis.

3.4. Characteristics of biochar pore structure

BET analyses of AB and WSB were carried out and compared, due to the obvious porous structure of AB. As shown in Table 1, there were significant differences in the specific surface area and pore size between AB and WSB. Upon pyrolysis which was activated by NaOH, the specific surface area of biochar increased drastically. The specific surface area of AB is 144 times as large as WSB. It was also larger than the activated carbon prepared from cattail fiber via chemical activation using phosphoric acid [25]. The activated carbon had a large surface area of $890.27 \text{ m}^2/\text{g}$ and its maximum adsorption capacities were 124.3 mg/g for 2,4-DCP adsorption and 172.4 mg/g for 2,4,6-trichlorophenol adsorption. Besides that, the pore volume of AB was also larger than that of WSB. In addition, the average pore

diameter decreased from 15.27 to 2.13 nm. In conclusion, AB had a mesopore structure with a large specific surface area. Previous literature has reported that HCl or NaOH treatment of biochar at room temperature can remove the ash, base soluble carbon, and blockages and improve the specific surface area of biochar to some extent and resulted in an enhanced performance in removing 1,2,4-trichlorobenzene and Cr(VI) [38,39]. Herein, the results suggested that the pyrolysis process with NaOH at high temperature played a better role in the significant increase in the specific surface area of AB.

The N_2 adsorption/desorption isotherms of WSB and AB are compared in Fig. 5. For WSB, there was no inflection point and lag ring in the relative pressure zone (Fig. 5a). The curve rose slowly at first and then had a sharp rise, indicating that it was a weak adsorbent. However, there was an inflection point in the adsorption/desorption isotherm curve of AB in the relative pressure zone (Fig. 5b). As the pressure increased, the adsorption amount quickly reached the balance value, indicating that the adsorbent had a strong adsorption performance. In conclusion, AB had a better adsorption performance than WSB and was therefore deemed as a stronger adsorbent.

The Barrett–Joyner–Halenda adsorption pore size distributions of WSB and AB are compared in Fig. 6. The pore sizes of WSB mainly ranged from 2 nm and 55 nm, indicating the presence of the mesopore structure. By comparison, AB had a smaller pore size than WSB. The pore sizes decreased to 2–10 nm, suggesting that AB was mainly consisted of mesopores and a few micropores. As expected, AB possessed relatively higher pore volume. These features explained why AB had a better adsorption performance than WSB, as revealed by the N_2 adsorption/desorption isotherms. It is expected that AB will exhibit an outstanding adsorption capacity in the removal of 2,4-DCP from water.

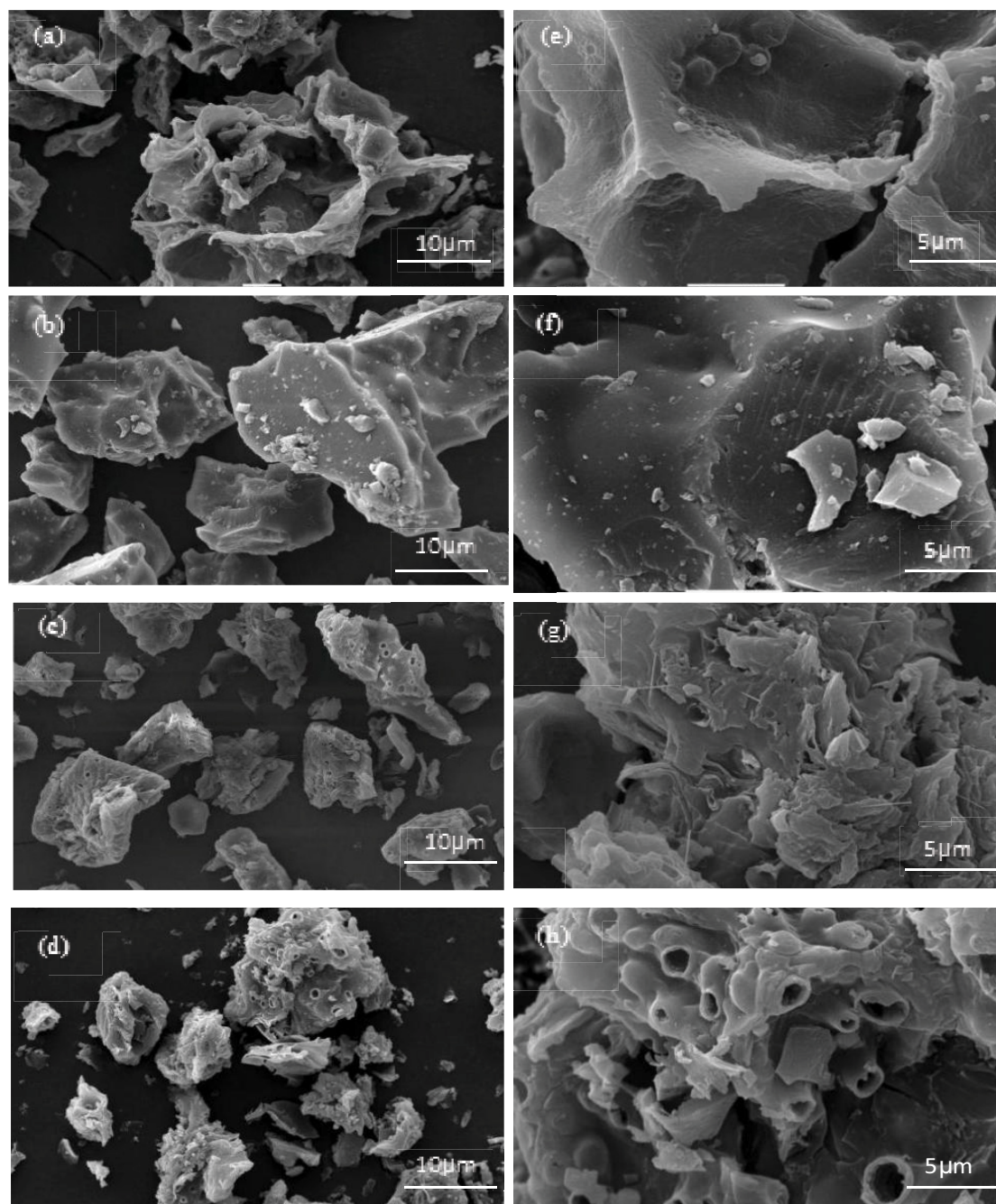


Fig. 4. SEM images of (a) WSB, (b) NB, (c) HB, (d) AB surface and (e) WSB, (f) NB, (g) HB, (h) AB cross-section.

Table 1
The pore structure parameters of WSB and AB

Sample	WSB	AB
Surface area (m^2/g)	7.87	1,138.74
Total pore volume (cm^3/g)	0.016	0.605
Average pore diameter (nm)	15.27	2.13
Total micropore volume (cm^3/g)	0.002	0.288
Total mesopore volume (cm^3/g)	0.014	0.317
$V_{\text{mesopore}}/V_{\text{micropore}}$	7	1.1

3.5. Adsorption kinetics

Fig. 7 shows the adsorption capacity of the biochar for 2,4-DCP with time while the initial concentration and the amount of the adsorbents were 0.2 g/L and 0.02 g, respectively. The adsorption proceeded rapidly in the first 60 min and then increased gradually. WSB reached the adsorption equilibrium after 120 min. The adsorption capacity of NB exceeded WSB after 120 min. HB and AB had both shown greater adsorption capacity than WSB. Especially for AB, the adsorption capacity reached 240.4 mg/g that was more than twice that of WSB which reached 106.7 mg/g. The

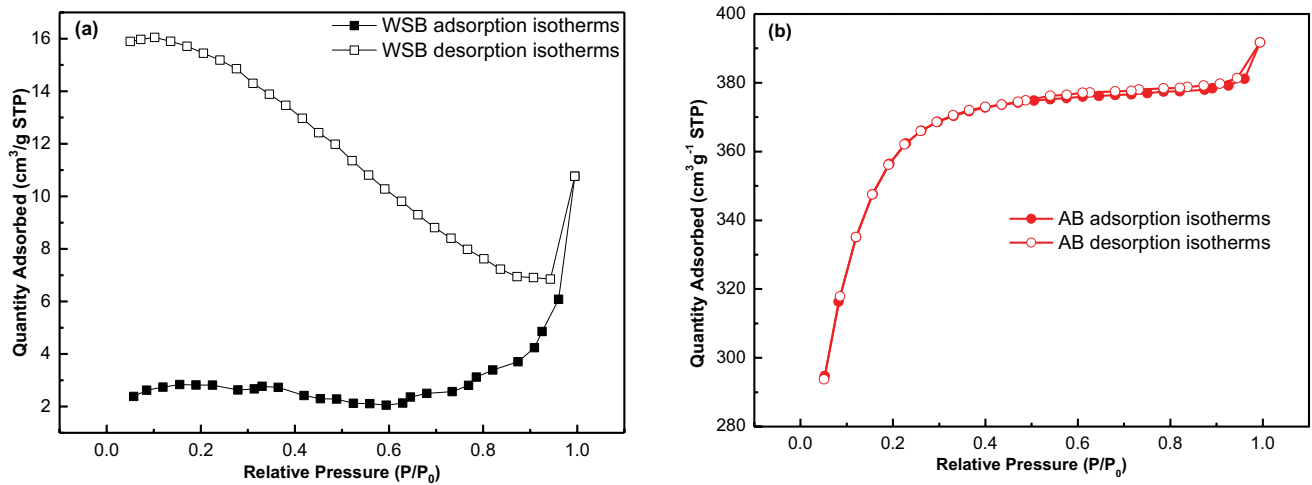


Fig. 5. N₂ adsorption–desorption isotherms of (a) WSB and (b) AB.

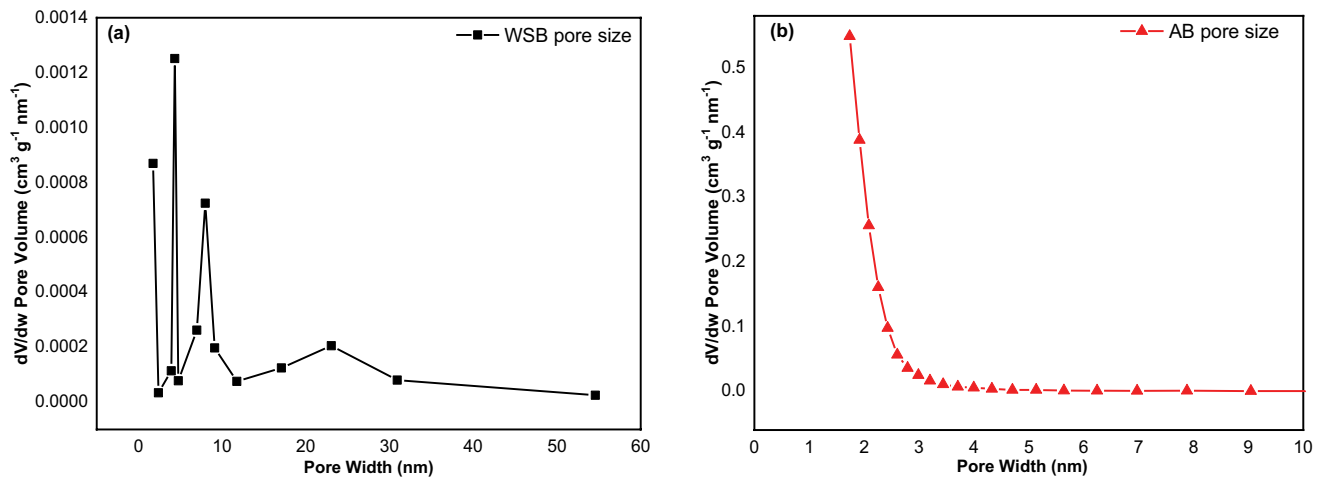


Fig. 6. The pore size distribution curves of (a) WSB and (b) AB.

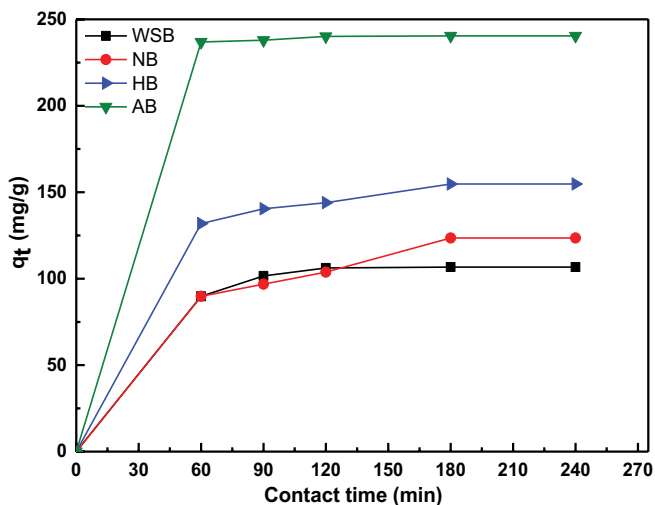


Fig. 7. Adsorption capacity of the biochar for 2,4-DCP.

significant increase could be attributed to the mesopore structure and large specific surface area of AB.

Under the conditions that the initial concentration and the amount of the adsorbents were 0.2 g/L and 0.02 g, respectively, removal efficiencies of the walnut shell-based biochars are compared in Fig. 8. The removal rates for 2,4-DCP by AB, HB, and NB were 2.3, 1.5, and 1.2 times that of WSB, respectively. AB had the most effective adsorption and its removal rate reached 96.5%. It suggested that the modification of WSB increased the adsorption effect of the biochar significantly. In addition, the removal rates of these biochars were also higher than the commercial activated carbon prepared from coconut shell which had a removal percentage of 23.11%, in 50 ppm of 2,4-DCP [40]. In other words, AB, HB, NB, and WSB possessed a removal rate 4.2, 2.7, 2.1, and 1.8 times as much as the commercial activated carbon, respectively.

The pseudo-first-order model, pseudo-second-order model, and intraparticle diffusion model were used to study the adsorption mechanism and to speculate on the kinetics of adsorption. The parameters are listed in Table 2.

Compared to the experimental result of the adsorption capacity (Q_e), the calculated values of q_e from the pseudo-first-order kinetics model were unreasonable and the values from the pseudo-second-order model were closer to Q_e . Furthermore, the corresponding correlation coefficients (R^2) of the pseudo-first-order kinetics and intraparticle diffusion equation were lower than those of the pseudo-second-order equation. In conclusion, the results showed that the adsorption followed the pseudo-second-order kinetic model, suggesting that chemisorption was primarily responsible.

Fig. 9 exhibits the pseudo-second-order adsorption kinetic equation fitting curves of the experimental data. The correlation coefficients (R^2) of the pseudo-second-order equation of AB and WSB were 0.999 and 0.997, respectively. The high correlation implied that the adsorption occurred via a chemisorption process and the adsorption mechanism maintained upon chemical modification. In addition, R^2 of NB and HB were 0.952 and 0.997, respectively, revealing that the primary adsorption was also chemisorption.

Additionally, the initial adsorption rate h (mg/g min) of 2,4-DCP by biochar could be obtained from the pseudo-second-order kinetic model, basing on Eq. (10) as follows:

$$h = k_2 q_e^2 \quad (10)$$

According to the main influencing factors of the pseudo-second-order kinetic equation, it can be inferred that

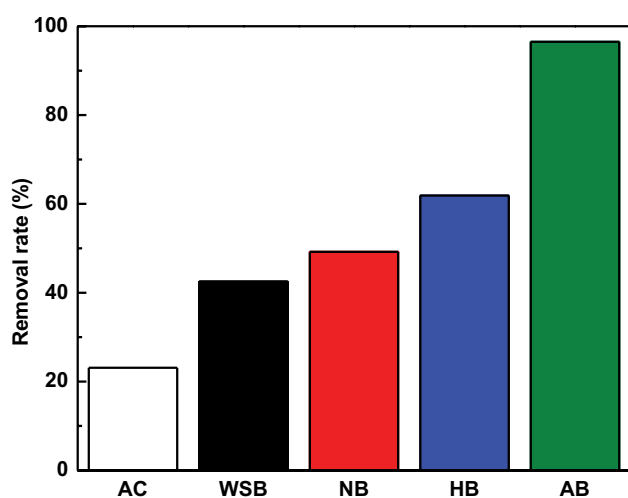


Fig. 8. Adsorption effect of commercial activated carbon and biochar before and after modification.

the adsorption process is affected by the chemical reaction/chemisorption rather than a physical process [31,41]. The initial adsorption rate h of AB increased to 76.69 mg/(g min), which was higher than WSB (Table 2).

3.6. Adsorption isotherm

Adsorption isotherms play an important role in the investigation of the adsorption mechanism. The adsorption isotherms of 2,4-DCP on biochars were studied and Freundlich and Langmuir models were used to fit the data and reveal the adsorption process, as presented in Fig. 10. The parameters of the Langmuir and Freundlich isotherm models were calculated based on the experimental data and shown in Table 3. The analysis showed that the Langmuir model had a higher R^2 value than the Freundlich model, indicating that the adsorption fit better into the Langmuir isotherm equation. It suggested that the adsorption of 2,4-DCP onto biochars was monolayer adsorption [32]. The R_L value ranged from 0–1 and the $1/n$ value were all within the range of 0–0.5, revealing that the adsorption process was favorable. $1/n$ value of AB was lower, which demonstrated the easier adsorption of 2,4-DCP on AB than on NB and HB.

3.7. Possible mechanism of adsorption for 2,4-DCP by AB

The adsorption of 2,4-DCP on biochar was a monolayer chemisorption process, as showed by the results from

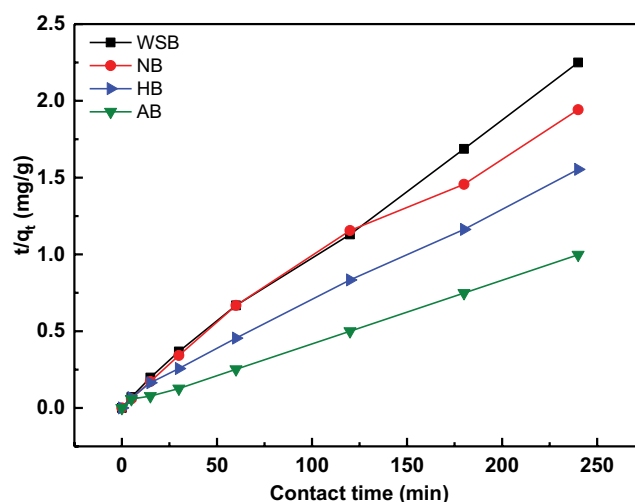


Fig. 9. Pseudo-second-order kinetic equation fitting curves.

Table 2
Isotherm parameters in adsorption of 2,4-DCP on biochar

Adsorbent	Pseudo-first-order				Pseudo-second-order				Intraparticle diffusion		
	Q_e (mg/g)	q_e (mg/g)	k_1 (g/mg min)	R^2	q_e (mg/g)	k_2 (g/mg min)	R^2	h (mg/g min)	C_i (mg/g)	k_{id} (g/mg min)	R^2
WSB	106.7	75.34	3.97×10^{-2}	0.937	109.2	1.60×10^{-3}	0.997	19.12	3.064	66.07	0.893
NB	148.7	175.14	1.93×10^{-2}	0.814	141.8	4.49×10^{-4}	0.952	9.03	4.665	61.66	0.750
HB	154.5	115.28	3.02×10^{-2}	0.760	158.7	7.96×10^{-4}	0.997	20.05	6.039	74.11	0.867
AB	240.4	55.85	3.46×10^{-2}	0.845	244.5	1.28×10^{-3}	0.999	76.69	7.976	143.20	0.370

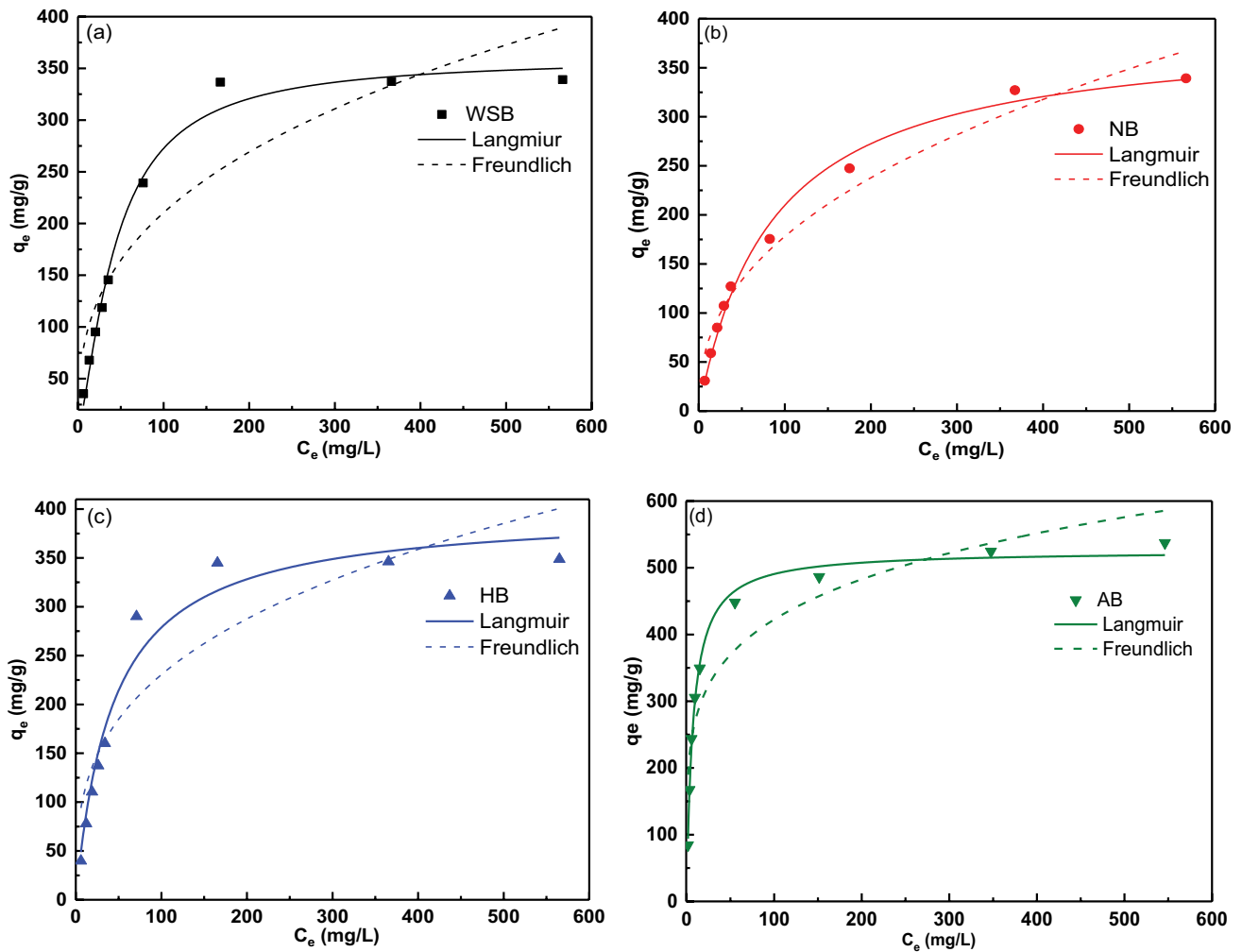


Fig. 10. Adsorption isotherms of 2,4-DCP on biochar (a) WSB, (b) NB, (c) HB, and (d) AB.

Table 3
Isotherm parameters of the biochar adsorption model before and after modification

Adsorbent	Langmuir				Freundlich		
	q_m (mg/g)	k_L (L/mg)	R_L	R^2	k_F (L/mg)	$1/n$	R^2
WSB	397.1978	0.0176	0.5450	0.9749	41.0023	0.3552	0.8509
NB	389.0785	0.0117	0.6329	0.9914	25.9837	0.4179	0.9655
HB	399.0204	0.0232	0.4464	0.9647	52.9795	0.3193	0.8145
AB	525.7792	0.1396	0.1191	0.993	174.2202	0.1924	0.8555

adsorption isotherm and kinetics. In order to further confirm the chemical interaction between biochar and 2,4-DCP, the infrared spectra of biochars before and after adsorption process are compared in Fig. 11 and a new peak at $1,621\text{ cm}^{-1}$ was observed, confirming the involvement of chemical bonding between 2,4-DCP and biochar during the adsorption process.

Besides the appearance of the new peak, the obvious peak of AB at $1,415\text{ cm}^{-1}$ attributable to aromatic rings disappeared after adsorption process, indicating the participation of the aromatic hydrocarbons and their derivatives in

the adsorption process. It was consistent with the previous research which reported that the aromatic hydrocarbons and their derivatives formed in biochars during pyrolysis and that the main adsorbed functional groups of biochars were benzene ring, $-\text{COOH}$, and $-\text{CH}_3$ for adsorption of aromatic pollutants [35,36]. It may be one of the reasons why AB has higher adsorption capacity than WSB which showed no band at $1,415\text{ cm}^{-1}$.

In addition, the high adsorption capacity of AB also resulted from the mesopore structure with larger specific surface area than WSB, because the larger surface exposed

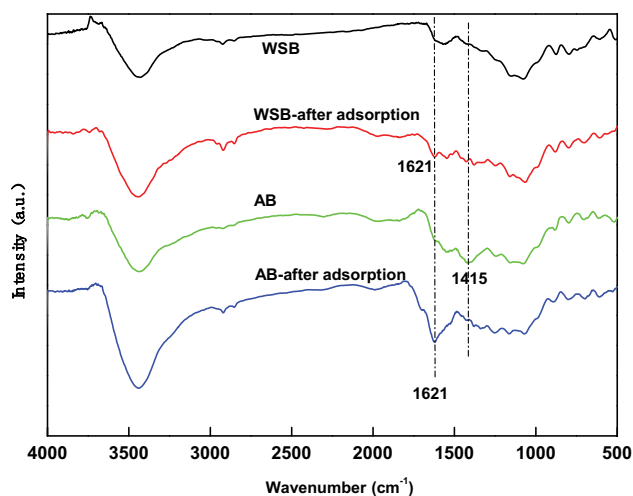


Fig. 11. FT-IR spectra of WSB and AB before and after adsorption of 2,4-DCP.

more aromatic adsorption sites for 2,4-DCP during the monolayer chemisorption process [38]. In conclusion, the aromatic hydrocarbons and their derivatives on the large surface of AB formed interaction with 2,4-DCP and remove 2,4-DCP from water.

4. Conclusions

Walnut shell-based biochars were effective adsorbents for the removal of 2,4-DCP and possessed higher removal rates than commercial activated carbon. The pyrolysis process of biochar with NaOH at high temperature significantly increased the specific surface area of AB and formed the aromatic hydrocarbons and their derivatives in AB. Due to these reasons, the alkali-activated biochar exhibited the highest removal rate and adsorption capacity which reached 96.5% and 240.4 mg/g, respectively. The adsorption of 2,4-DCP on AB and WSB was best described by the pseudo-second-order kinetic adsorption equation and best fitted by the Langmuir isotherm model. This present research provides a theoretical basis for the future utilization of walnut shells and provides an alternative solution for chlorophenol removal from wastewater.

Acknowledgments

This work was supported by Key Laboratory of Advanced Textile Materials and Manufacturing Technology (Ministry of Education of China); Zhejiang Provincial Key Laboratory of Fiber Materials and Manufacturing Technology (Zhejiang Sci-Tech University) (2019002); and the 12th Postgraduate Education Innovation Fund of Wuhan Institute of Technology (CX2020289).

References

[1] C.S.G.P. Queirós, S. Cardoso, A. Lourenço, J. Ferreira, I. Miranda, M.J.V. Lourenço, H. Pereira, Characterization of walnut, almond, and pine nut shells regarding chemical composition and extract composition, *Biomass Convers. Biorefin.*, 10 (2020) 175–188.

[2] B. Zhang, P. Jin, H. Qiao, T. Hayat, A. Alsaedi, B. Ahmad, Exergy analysis of Chinese agriculture, *Ecol. Ind.*, 105 (2019) 279–291.

[3] S. Zhou, Y. Wei, B. Li, H. Wang, Cleaner recycling of iron from waste copper slag by using walnut shell char as green reductant, *J. Cleaner Prod.*, 217 (2019) 423–431.

[4] J. Wei, G. Liang, J. Alex, T. Zhang, C. Ma, Research progress of energy utilization of agricultural waste in China: bibliometric analysis by citespace, *Sustainability*, 12 (2020) 812–834.

[5] K.U. Mohammad, N. Abu, Walnut shell powder as a low-cost adsorbent for methylene blue dye: isotherm, kinetics, thermodynamic, desorption and response surface methodology examinations, *Sci. Rep.*, 10 (2020) 7953, doi: 10.1038/s41598-020-64745-3.

[6] C. Kang, L. Zhu, Y. Wang, Y. Wang, K. Xiao, T. Tian, Adsorption of basic dyes using walnut shell-based biochar produced by hydrothermal carbonization, *Chem. Res.*, 34 (2018) 622–627.

[7] V. Halysh, O. Sevastyanova, A.V. Riazanova, B. Pasalskiy, T. Budnyak, M.E. Lindström, M. Kartel, Walnut shells as a potential low-cost lignocellulosic sorbent for dyes and metal ions, *Cellulose*, 25 (2018) 4729–4742.

[8] D. Mohan, A. Sarswat, Y.S. Ok, C.U. Pittman Jr., Organic and inorganic contaminants removal from water with biochar, a renewable, low cost and sustainable adsorbent – a critical review, *Bioresour. Technol.*, 160 (2014) 191–202.

[9] I. Anastopoulos, I. Pashalidis, A. Hosseini-Bandegharaei, D.A. Giannakoudakis, A. Robalds, M. Usman, L.B. Escudero, Y. Zhou, J.C. Colmenares, A. Núñez-Delgado, E.C. Lima, Agricultural biomass/waste as adsorbents for toxic metal decontamination of aqueous solutions, *J. Mol. Liq.*, 295 (2019) 111684, doi: 10.1016/j.molliq.2019.111684.

[10] M.A. Khan, A.A. Alqadami, M. Otero, M.R. Siddiqui, Z.A. Alothman, I. Alsohaimi, M. Rafatullah, A.E. Hamedelnie, Heteroatom-doped magnetic hydrochar to remove post-transition and transition metals from water: synthesis, characterization, and adsorption studies, *Chemosphere*, 218 (2019) 1089–1099.

[11] H. Shang, Y. Li, J. Liu, Y. Wan, Y. Feng, Y. Yu, Preparation of nitrogen doped magnesium oxide modified biochar and its sorption efficiency of lead ions in aqueous solution, *Bioresour. Technol.*, 314 (2020) 123708, doi: 10.1016/j.biortech.2020.123708.

[12] Z. Fang, Y. Gao, N. Bolan, S.M. Shaheen, S. Xu, X. Wu, X. Xu, H. Hu, J. Lin, F. Zhang, J. Li, J. Rinklebe, H. Wang, Conversion of biological solid waste to graphene-containing biochar for water remediation: a critical review, *Chem. Eng. J.*, 390 (2020) 124611, doi: 10.1016/j.cej.2020.124611.

[13] Z. Yu, L. Zhou, Y. Huang, Z. Song, W. Qiu, Effects of a manganese oxide-modified biochar composite on adsorption of arsenic in red soil, *J. Environ. Manage.*, 163 (2015) 155–162.

[14] Z. Ding, X. Hu, Y. Wan, S. Wang, B. Gao, Removal of lead, copper, cadmium, zinc, and nickel from aqueous solutions by alkali-modified biochar: batch and column tests, *J. Ind. Eng. Chem.*, 33 (2016) 239–245.

[15] S. Batool, M. Idrees, M. Ahmad, M. Ahmad, Q. Hussain, A. Iqbal, J. Kong, Design and characterization of a biomass template/SnO₂ nanocomposite for enhanced adsorption of 2,4-dichlorophenol, *Environ. Res.*, 181 (2020) 108955, doi: 10.1016/j.envres.2019.108955.

[16] N.S. Trivedi, R.A. Kharkar, S.A. Mandavgane, 2,4-Dichlorophenoxyacetic acid adsorption on adsorbent prepared from groundnut shell: effect of preparation conditions on equilibrium adsorption capacity, *Arabian J. Chem.*, 12 (2019) 4541–4549.

[17] Z. Liu, Q. Qin, Z. Hu, L. Yan, U. Jeong, Y. Xu, Adsorption of chlorophenols on polyethylene terephthalate microplastics from aqueous environments: kinetics, mechanisms and influencing factors, *Environ. Pollut.*, 265 (2020) 114926, doi: 10.1016/j.envpol.2020.114926.

[18] M. Czaplicka, Sources and transformations of chlorophenols in the natural environment, *Sci. Total Environ.*, 322 (2004) 21–39.

[19] P.V. Aken, V. Rob, J. Degreuve, R. Dewil, A pilot-scale coupling of ozonation and biodegradation of 2,4-dichlorophenol-containing wastewater: the effect of biomass acclimation

- towards chlorophenol and intermediate ozonation products, *J. Cleaner Prod.*, 161 (2017) 1432–1441.
- [20] N. Tong, J. Yuan, H. Xu, S. Huang, C. Sun, X. Wen, Y. Zhang, Effects of 2,4,6-trichlorophenol on simultaneous nitrification and denitrification: performance, possible degradation pathway and bacterial community structure, *Bioresour. Technol.*, 290 (2019) 121757, doi: 10.1016/j.biortech.2019.121757.
- [21] P.J. Dorathi, P. Kandasamy, Dechlorination of chlorophenols by zero valent iron impregnated silica, *J. Environ. Sci.*, 24 (2012) 765–773.
- [22] X. Cheng, H. Guo, Y. Zhang, Y. Liu, H. Liu, Y. Yang, Oxidation of 2,4-dichlorophenol by non-radical mechanism using persulfate activated by Fe/S modified carbon nanotubes, *J. Colloid Interface Sci.*, 469 (2016) 277–286.
- [23] W. Liu, D. Ren, J. Wu, Z. Wang, S. Zhang, X. Zhang, X. Gong, Adsorption behavior of 2,4-DCP by rice straw biochar modified with CTAB, *Environ. Technol.*, 42 (2020) 3797–3806.
- [24] A. Allwar, S. Syamsurizal, Removal of 2-chlorophenol using rice husk activated carbon prepared by $ZnCl_2/H_3PO_4$ activation, *Orient J. Chem.*, 33 (2017) 2386–2393.
- [25] L. Ren, J. Zhang, Y. Li, C. Zhang, Preparation and evaluation of cattail fiber-based activated carbon for 2,4-dichlorophenol and 2,4,6-trichlorophenol removal, *Chem. Eng. J.*, 168 (2011) 553–561.
- [26] W.J. Liu, F.X. Zeng, H. Jiang, X.S. Zhang, Preparation of high adsorption capacity bio-chars from waste biomass, *Bioresour. Technol.*, 102 (2011) 8247–8252.
- [27] D. Kalderis, B. Kayan, S. Akay, E. Kulaksız, B. Gözmen, Adsorption of 2,4-dichlorophenol on paper sludge/wheat husk biochar: process optimization and comparison with biochars prepared from wood chips, sewage sludge and hog fuel/demolition waste, *J. Environ. Chem. Eng.*, 5 (2017) 2222–2231.
- [28] Y. Wu, B. Chen, Effect of fulvic acid coating on biochar surface structure and sorption properties towards 4-chlorophenol, *Sci. Total Environ.*, 691 (2019) 595–604.
- [29] X. Song, P. Ning, C. Wang, K. Li, L. Tang, X. Sun, H. Ruan, Research on the low temperature catalytic hydrolysis of COS and CS₂ over walnut shell biochar modified by Fe-Cu mixed metal oxides and basic functional groups, *Chem. Eng. J.*, 314 (2017) 418–433.
- [30] S. Chowdhury, P. Saha, Adsorption kinetic modeling of safranin onto rice husk biomatrix using pseudo-first- and pseudo-second-order kinetic models: comparison of linear and non-linear methods, *Clean-Soil, Air, Water*, 39 (2011) 274–282.
- [31] H.M. Jang, S. Yoo, Y.-K. Choi, S. Park, E. Kan, Adsorption isotherm, kinetic modeling and mechanism of tetracycline on *Pinus taeda*-derived activated biochar, *Bioresour. Technol.*, 259 (2018) 24–31.
- [32] S. Azizian, S. Eris, L.D. Wilsn, Re-evaluation of the century-old Langmuir isotherm for modeling adsorption phenomena in solution, *Chem. Phys.*, 513 (2018) 99–104.
- [33] P. Pachfule, D. Shinde, M. Majumder, Q. Xu, Fabrication of carbon nanorods and graphene nanoribbons from a metal-organic framework, *Nat. Chem.*, 8 (2016) 718–724.
- [34] A. Ghosh, C.d.A. Razzino, A. Dasgupta, K. Fujisawa, L.H.S. Vieira, S. Subramanian, R.S. Costa, A.O. Lobo, O.P. Ferreira, J. Robinson, M. Terrones, H. Terrones, B.C. Viana, Structural and electrochemical properties of babassu coconut mesocarp-generated activated carbon and few-layer graphene, *Carbon*, 145 (2019) 175–186.
- [35] A. Krzyszczyk, M.P. Dybowski, B. Czech, Formation of polycyclic aromatic hydrocarbons and their derivatives in biochars: the effect of feedstock and pyrolysis conditions, *J. Anal. Appl. Pyrolysis*, 160 (2021) 105339–105349.
- [36] X. Zhou, L. Shi, T.B. Moghaddam, M. Chen, S. Wu, X. Yuan, Adsorption mechanism of polycyclic aromatic hydrocarbons using wood waste-derived biochar, *J. Hazard. Mater.*, 425 (2022) 128003–128019.
- [37] R.J. Evans, T.A. Milne, M.N. Soltys, Direct mass-spectrometric studies of the pyrolysis of carbonaceous fuels: III. Primary pyrolysis of lignin, *J. Anal. Appl. Pyrolysis*, 9 (1986) 207–236.
- [38] X. Shang, L. Yang, D. Ouyang, B. Zhang, W. Zhang, M. Gu, J. Li, M. Chen, L. Huang, L. Qian, Enhanced removal of 1,2,4-trichlorobenzene by modified biochar supported nanoscale zero-valent iron and palladium, *Chemosphere*, 249 (2020) 126518–126528.
- [39] H.R. Dong, J.M. Deng, Y.K. Xie, C. Zhang, Z. Jiang, Y.J. Cheng, K.J. Hou, G.M. Zeng, Stabilization of nanoscale zero-valent iron (nZVI) with modified biochar for Cr(VI) removal from aqueous solution, *J. Hazard. Mater.*, 332 (2017) 79–86.
- [40] S.M. Anisuzzaman, C.G. Joseph, Y.H. Taufiq-Yap, D. Krishnaiah, V.V. Tay, Modification of commercial activated carbon for the removal of 2,4-dichlorophenol from simulated wastewater, *J. King Saud Univ. Sci.*, 27 (2015) 318–330.
- [41] Q.S. Liu, T. Zheng, P. Wang, J.P. Jiang, N. Li, Adsorption isotherm, kinetic and mechanism studies of some substituted phenols on activated carbon fibers, *Chem. Eng. J.*, 157 (2010) 348–356.